AIP | The Journal of Chemical Physics

Molecular dynamics study of nanoparticle stability at liquid interfaces: Effect of nanoparticle-solvent interaction and capillary waves

David L. Cheung

Citation: J. Chem. Phys. **135**, 054704 (2011); doi: 10.1063/1.3618553
View online: http://dx.doi.org/10.1063/1.3618553
View Table of Contents: http://jcp.aip.org/resource/1/JCPSA6/v135/i5
Published by the American Institute of Physics.

Molecular dynamics study of nanoparticle stability at liquid interfaces: Effect of nanoparticle-solvent interaction and capillary waves

David L. Cheung[a)]
Department of Chemistry and Centre for Scientific Computing, University of Warwick, Coventry CV4 7AL, United Kingdom

(Received 4 March 2011; accepted 6 July 2011; published online 1 August 2011)

While the interaction of colloidal particles (sizes in excess of 100 nm) with liquid interfaces may be understood in terms of continuum models, which are grounded in macroscopic properties such as surface and line tensions, the behaviour of nanoparticles at liquid interfaces may be more complex. Recent simulations [D. L. Cheung and S. A. F. Bon, Phys. Rev. Lett. **102**, 066103 (2009)] of nanoparticles at an idealised liquid-liquid interface showed that the nanoparticle-interface interaction range was larger than expected due, in part, to the action of thermal capillary waves. In this paper, molecular dynamics simulations of a Lennard-Jones nanoparticle in a binary Lennard-Jones mixture are used to confirm that these previous results hold for more realistic models. Furthermore by including attractive interactions between the nanoparticle and the solvent, it is found that the detachment energy decreases as the nanoparticle-solvent attraction increases. Comparison between the simulation results and recent theoretical predictions [H. Lehle and M. Oettel, J. Phys. Condens. Matter **20**, 404224 (2008)] shows that for small particles the incorporation of capillary waves into the predicted effective nanoparticle-interface interaction improves agreement between simulation and theory.
 [doi:10.1063/1.3618553]

I. INTRODUCTION

The adsorption of nanometer-sized particles, including nanoparticles, polymers or dendrimers and proteins, at soft interfaces has attracted much scientific interest[1] and is central to a number of emerging technologies. Adhesion at air-water and oil-water interfaces potentially provides an elegant method for the preparation of dense, ordered nanoparticle structures,[2] and the modification of interfacial properties by the adsorption of nanoparticles may be used to stabilise micrometer-scale structures such as nanoparticle-armoured fluid droplets[3] or phase-arrested gels.[4] As well as synthetic nanoparticles the behaviour of biological objects, such as proteins[5] or virus capsids,[6] at liquid interfaces have also been the subject of investigation.

Due to the experimental interest in these systems, the behaviour of nanoparticles at liquid interfaces has been studied theoretically, both using analytic and semi-analytic theories and molecular simulations. The adhesion of solid particles to liquid interfaces has long been understood as a result of particle wettability and changes in interfacial area.[7,8] The theory of colloidal adhesion on liquid interfaces has been thoroughly developed, including both the effect of particle fluid surface tensions[9,10] and line tension.[11] These models are typically derived from considering colloidal (200–1000 nm) sized particles and so are grounded in macroscopic quantities such as surface and line tensions, and neglect microscopic phenomena such as capillary waves. One common model is the Pieranski approximation[8] in which the free energy is given simply in terms of changes to the interfacial area (A_{AB}) and the area of the nanoparticle in contact with the two fluid components (A_{iN}) as

$$F(z_c) = -\gamma_{AB}A_{AB} + \gamma_{AN}A_{AN} + \gamma_{BN}A_{BN} = \pi\gamma_{AB}z_c^2 + 2\pi R_c^2(\gamma_{AN} - \gamma_{BN})(1 - z_c/R_c), \quad (1)$$

where z_c is the distance between the interface and the colloid centre, γ_{AB} is the A-B interfacial tension, γ_{iN} is the surface tension between the nanoparticle and fluid component i and R_c is the nanoparticle radius. This was then extended by Aveyard and Clint (AC) to include line tension,[11] giving

$$F(z_c) = \pi\gamma_{AB}z_c^2 + 2\pi R_c^2(\gamma_{AN} - \gamma_{BN})(1 - z_c/R_c) + 2\pi\tau R_c\sqrt{1 - (z_c/R_c)^2}. \quad (2)$$

Recently these analytic theories have been extended to consider the effect of capillary waves on the nanoparticle-interface interaction[12] and interface mediated nanoparticle-nanoparticle interactions.[13,14]

The adsorption of nanoparticles on liquid interfaces has also been studied using molecular simulations. In pioneering work, Bresme and Quirke employed molecular dynamics simulations to study the effect of line tension on the stability of nanoparticles at liquid interfaces.[15–17] More recently the interaction potential between a nanoparticle and a liquid interface was determined using Monte Carlo or molecular dynamics simulations, for uniform,[18] Janus (amphiphilic),[19] and polymer-grafted nanoparticles.[20] Simulations have also been used to study the interactions between adsorbed nanoparticles,[21] self-assembly of nanoparticles at liquid-liquid interfaces,[22] and nanoparticle diffusion at interfaces.[23,24] Density functional theory has also been recently used to study the interaction and wetting behaviour of nanoparticles at fluid interfaces.[25,26]

a)Electronic mail: david.cheung@warwick.ac.uk.

In some recent Monte Carlo (MC) simulations of the Widom-Rowlinson mixture,[27] the nanoparticle-interface interaction was found to be significantly longer ranged than predicted by continuum theories[18] due to the neglect of microscopic phenomena, such as capillary waves. Recently a number of other effects that are neglected by macroscopic models on the behaviour of nanoparticles at liquid interfaces have been considered (although this has largely focused on interactions between nanoparticles absorbed at interfaces rather than interactions between interfaces and nanoparticles). These include capillary forces arising due to deformation of the interface due to adsorbed particles (e.g., meniscus formation[28]), which have been shown to lead to attractive forces between adsorbed nanoparticles but to an increase in the free energy barrier in the analogous case of nanoparticle-membrane penetration.[29] Changes to the solvent structure around the nanoparticle may also lead to interactions between nanoparticles in solution and to interactions between nanoparticle and interfaces or surfaces (e.g., hydration or depletion forces). The effect of specific nanoparticle-solvent interactions, such as van der Waals and electrostatic forces, may also be a significant factor in determining the interfacial behaviour of nanoparticles, the latter of which may be particularly important in nanoparticle near interfaces in electrolytic solutions or ionic fluids. The effect of these and other phenomena have been recently reviewed.[1,30] Due to its simple form the Widom-Rowlinson model used in the previous work, however, may be regarded as somewhat singular and unrepresentative of experimental systems; in particular the interfacial tension of the Widom-Rowlinson mixture studied in the previous work was significantly smaller than that of a typical liquid mixture. It is then natural to ask how applicable these findings are to other, more realistic, fluid models.

In this paper, the interaction between a nanoparticle and a liquid interface, modelled in this case by Lennard-Jones (LJ) interactions, is studied using molecular dynamics simulations. While the Wang-Landau MC simulations[31] that were used in previous work[18,19] may be applied in this case, they may be inefficient when applied to complex molecular systems, and in the case of very large free energy barriers the time required to determine a converged weight function may be prohibitively long. Molecular dynamics simulations are more easily generalised to complex systems and may be easily parallelised to take advantage of modern parallel computers. Free energy profiles may be determined using methods, such as umbrella sampling,[32] steered molecular dynamics,[33] metadynamics[34] or adaptive biasing force,[35] the latter two being conceptually similar to the Wang-Landau MC methodology used previously.

In this paper, molecular dynamics simulations are used to study the stability of a spherical nanoparticle at a model liquid-liquid interface. The free energy profile was determined using umbrella sampling, a simple and robust method for this purpose. As well as testing the validity of the results of Ref. 18 for more realistic fluids, the effect of attractive nanoparticle-solvent interactions and the effect of capillary waves on the interaction will be examined. Details of the computational model and methodology are given in Sec. II, the results of the simulations are presented and discussed in Sec. III, while Sec. IV gives some conclusions and avenues for further work.

II. MODEL AND METHODOLOGY

The solvent is modelled as a two-component fluid, interacting through a cut and shifted Lennard-Jones potential,

$$V_S(r) = \begin{cases} 4\epsilon\left[\left(\frac{\sigma}{r}\right)^{12} - \left(\frac{\sigma}{r}\right)^{6}\right] - V_{cut}, & r \le r_{cut}, \\ 0, & r > r_{cut}, \end{cases} \tag{3}$$

where $V_{cut} = 4\epsilon[(\sigma/r_{cut})^{12} - (\sigma/r_{cut})^6]$ and $r_{cut} = 2.5\sigma$ for like particles and $r_{cut} = \sqrt[6]{2}\sigma$ for unlike particles (i.e., the potential is truncated and shifted at the potential minima). In comparison to the Widom-Rowlinson model used in the previous work, this model incorporates explicit interactions between identical solvent particles, including attractive, dispersion forces, which should give a more representative, though still simplified, model of a liquid mixture. For the densities studied in this paper ($\rho\sigma^3 \ge 0.50$), this mixture phase separates into distinct A and B rich regions. The nanoparticle-solvent interaction is taken to be a modified, expanded LJ interaction,

$$V_{SN}(r) = \begin{cases} 4\epsilon\left[\left(\frac{\sigma}{r-\Delta}\right)^{12} - \left(\frac{\sigma}{r-\Delta}\right)^{6}\right] - V_{cut} + \epsilon - \epsilon', & r - \Delta \le \sqrt[6]{2}, \\ 4\epsilon'\left[\left(\frac{\sigma}{r-\Delta}\right)^{12} - \left(\frac{\sigma}{r-\Delta}\right)^{6}\right] - V_{cut}, & \sqrt[6]{2} < r - \Delta \le r_{cut}, \\ 0, & r - \Delta > r_{cut}, \end{cases} \tag{4}$$

where $\Delta = (\sigma_N - \sigma)/2$ and $\sigma_N = 2R_c$ is the nanoparticle diameter. The effect of the parameter Δ is to shift the separation at which the interaction potential goes to infinity, giving the nanoparticle at non-zero size. It should be noted that this potential represents the nanoparticle as a single interaction and is similar to potentials used in previous studies.[15–17,21] This potential is a modification of the Lennard-Jones interaction to a particle of non-zero size. More sophisticated potentials explicitly representing the interaction of a superposition of pair potentials of atoms in a nanoparticle, may be found by integrating the Lennard-Jones potential over the volume of the nanoparticle.[36,37] Despite the difference in functional forms between the potential above (Eq. (4)) and that given in Ref. 36, they exhibit similar variation with nanoparticle-solvent separation, indicating that Eq. (4) provides a good approximation to a superposition of pair inter-

actions. Nanoparticles of radii $2.5\sigma \leq R_c \leq 4\sigma$ were studied. The parameter ϵ' is used to modulate the strength of the nanoparticle-solvent attraction; for $\epsilon' = 0$ this reduces to a purely repulsive interaction (equivalent to an expanded Weeks-Chandler-Anderson (WCA) interaction) and for $\epsilon' = \epsilon$ this is equivalent to a normal expanded LJ interaction. The plots of this potential for the values of ϵ' studied are shown in Fig. 1. This choice of this potential was motivated by the desire to vary the attractive part of the potential while holding the repulsive core constant, allowing a smooth interpolation between a purely repulsive potential and those with a finite attraction. It should be noted that this model is not intended to be representative of a specific experimental system and in particular the choice of identical interactions between the particle and both solvent components (neutral wetting) is unlike most commonly studied systems. However, it should be noted that systems with a contact angle $\theta \sim \pi/2$ can be realized experimentally[10] and recent simulations have shown that the behaviour of particles with different interactions between the solvent components are qualitatively similar to those with identical interactions.[19] The Lennard-Jones parameters for the solvent define the usual set of reduced units; in particular the temperature $T^* = \epsilon/k_B$, mass m^*, and number density $\rho^* = N\sigma^3/V$.

The free energy profile or potential of mean force is determined using umbrella sampling.[32] The nanoparticle z coordinate (z_c) is constrained at a series of points z_i using a harmonic potential,

$$V_i(z_c) = \tfrac{1}{2}k_i(z_c - z_i)^2, \tag{5}$$

where k_i is the force constant (with $\beta\sigma^2 k = 5 - 20$). For each z_i, the (biased) probability distribution $\mathcal{P}_i(z_c)$ is determined and the final (unbiased) probability distribution $\mathcal{P}(z)$ is determined using weighted histogram analysis.[38] For each value of ρ, R_c, and ϵ' 2.5×10^6 MD steps (including 0.5×10^6 equilibration steps) were performed for each z_i. In order to estimate errors in the free energy profiles, each of these simulation runs was divided into four subruns with the full analysis performed on these separately.

All simulations were performed using the LAMMPS simulation package[39] in the NVT ensemble,with $T^* = 1$. Temperature was controlled using a Nose-Hoover thermostat.[40] A time step of $\delta t = 0.005t^*$ (where $t^* = \sqrt{m^*\sigma^2/\epsilon}$) was used. In order to localise the interface in the centre of the simulation cell repulsive walls were placed in the z direction, with periodic boundaries in the x and y directions. The average z position of the interface is typically $|\bar{z}_{inter}| \leq 0.004\sigma$ (with a typical standard deviation $\sim 0.04\sigma$), where the cell centre defined is to be at $z = 0$. This allows the nanoparticle-interface separation to be approximated by the nanoparticle z coordinate (z_c). For comparison with continuum theory simulations without nanoparticles were used to calculate the interfacial tension using the virial expression,[41]

$$\gamma_{AB} = \int dz \left[P_{zz}(z) - \frac{P_{xx}(z) + P_{yy}(z)}{2} \right], \tag{6}$$

where $P_{ii}(z)$ are the diagonal components of the pressure tensor. The values of γ_{AB} are given in Table I. As most experiments are performed under constant pressure rather than constant volume conditions also presented in Table I are the average pressures for the different systems studied.

TABLE I. Lateral box lengths (note $L_z = 2L_x$), pressure, and interfacial tensions for the studied systems.

ρ^*	L_x/σ	$\beta\sigma^3 P$	$\beta\sigma^2\gamma_{AB}$
0.50	20	0.14	0.479
0.60	18.82	0.35	0.917
0.69	17.96	0.90	1.498

III. RESULTS

A. Effective nanoparticle-interface interaction

The free energy for the purely repulsive ($\epsilon' = 0$) nanoparticles are shown in Fig. 1. The free energy profiles have a minimum at $z_c = 0$ and then rise to a maximum some distance from the interface. As in previous work the range of the effective interaction is significantly larger than the particle radius caused by the broadening of the interface due to capillary waves. On increasing ρ the interaction range decreases due to the damping of the capillary wave amplitude with increase in γ_{AB}. In most cases, the effective potential increases monotonically towards the bulk value. For the $R_c = 4\sigma$ at $\rho^* = 0.69$, however, a small barrier appears at $z_c \approx 6.1\sigma$, presumably due to deformation of the interface by the nanoparticle, which would be washed out due to interface fluctuations when the particle size is smaller or interfacial tension is lower. The height of this barrier, relative to the particle in bulk solvent is $\sim 2k_BT$. Recent experimental studies[42] on TEG-stabilised gold nanoparticles have also observed an activation barrier of $\sim 2k_BT$ (it should be noted that due to the differences between the simulated and experimental systems the agreement between the barrier heights in the two cases is likely to be fortuitous), which was attributed to electrostatic forces or rearrangement of attached chains. As the present system has neither of these, this work demonstrates that such a barrier may also arise due to capillary effects.[29]

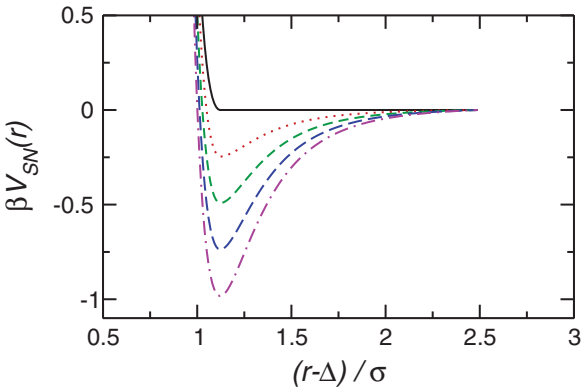

FIG. 1. Nanoparticle-solvent interaction potentials (Eq. (4)) with $\beta\epsilon' = 0$ (solid, black), $\beta\epsilon' = 0.25$ (dotted, red), $\beta\epsilon' = 0.50$ (dashed, green), $\beta\epsilon' = 0.75$ (long dashed, blue), and $\beta\epsilon' = 1$ (dotted-dashed, magenta). Solvent-solvent interaction (Eq. (3)) corresponds to $\Delta = 0$ and $\beta\epsilon' = 1$ and $\beta\epsilon' = 0$ for like (A-A and B-B) and unlike (A-B) interactions, respectively.

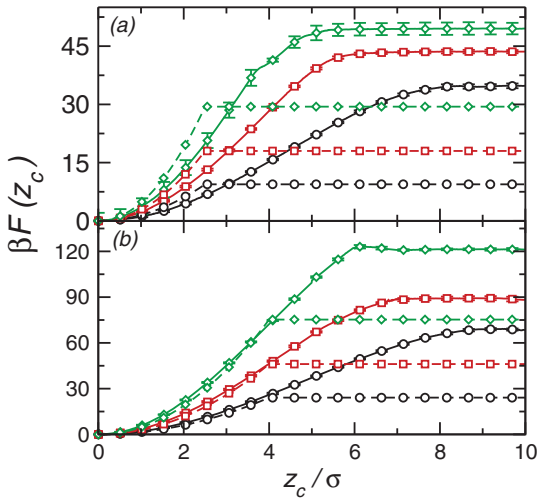

FIG. 2. (a) Free energy profile for $R_c = 2.5\sigma$ nanoparticle ($\epsilon' = 0$) at solvent density $\rho^* = 0.50$ (circles, black), $\rho^* = 0.60$ (squares, red), and $\rho^* = 0.69$ (diamonds, green). Solid line shows simulation results, dashed lines Pieranski approximation. (b) Free energy profiles for $R_c = 4.0\sigma$ nanoparticle ($\epsilon' = 0$). Symbols as in (a).

Also shown in Fig. 2 are the predicted effective potentials from the Pieranski approximation. As the nanoparticle-solvent interaction is identical for both components $\gamma_{AN} = \gamma_{BN}$ so Eq. (1) reduces to

$$F(z_c) = \pi \gamma_{AB} z_c^2. \tag{7}$$

As in the previous work, this underestimates both the height of the barrier and also the interaction range. The underestimation of the range arises due to its assumption of a sharp, flat interface (neglect of interface fluctuations). It is interesting to note that for the larger particles ($R_c = 4\sigma$) the simulation and Pieranski curves are in good agreement for the region $z \leq R_c$.

The detachment energies ΔF as a function of R_c are shown in Fig. 3. The values of ΔF are in the range expected for (10–100 $k_B T$) nanometer-sized particles[43] and are approximately an order of magnitude larger than those obtained for the Widom-Rowlinson model.[18] Such a difference may be expected as the interfacial tension of the Widom-Rowlinson model is up to an order of magnitude lower to those obtained in this work. The present ΔF is similar to those recently

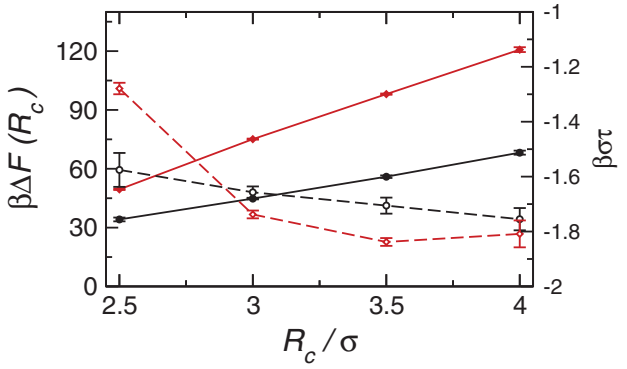

FIG. 3. Detachment energy and line tension against R_c for $\rho^* = 0.50$ (circles, black) and $\rho^* = 0.69$. Circles denote $\rho^* = 0.50$, diamonds $\rho^* = 0.69$, ΔF denoted by filled symbols (solid lines), and τ denoted by open symbols (dashed lines).

TABLE II. Detachment free energies calculated from simulation (ΔF_{sim}) and using the Pieranski approximation (Eq. (7)). $\beta \Delta F_{\text{Pier}}$ refers to detachment energy calculated using R_c, while $\beta \Delta F_{\text{Pier}}^{corr}$ denotes detachment energy calculated using corrected R_c found from the solvent density distribution.

ρ^*	R_c / σ	$\beta \Delta F_{sim}$	$\beta \Delta F_{\text{Pier}}$	$\Delta F_{\text{Pier}}^{corr}$
0.50	2.5	34.82	9.42	12.66
0.50	4.0	69.21	24.11	30.29
0.60	2.5	43.92	18.01	24.23
0.60	4.0	89.39	46.10	55.77
0.69	2.5	50.05	29.41	39.58
0.69	4.0	121.71	75.30	91.11

obtained for polymer grafted nanoparticles[20] and from experimental measurements of gold nanoparticles.[42] The detachment energy (ΔF) increases with particle radius. It is noticeable that this appears to scale approximately linearly with R_c rather than quadratically as would be expected from the Pieranski approximation. This linear dependence may arise due to a significant line tension. The line tension is difficult to calculate, but it may be estimated from the difference between the detachment energies from simulation and Pieranski approximation,[15]

$$\tau = -\frac{\Delta F_{sim} - \pi R_c^2 \gamma_{AB}}{2\pi R_c}. \tag{8}$$

In all cases (Table II) $\Delta F_{sim} > \pi R_c^2 \gamma_{AB}$, indicating that τ is negative, in agreement with previous studies.[16,18] For $\rho^* = 0.50$ τ decreases monotonically with R_c. For $\rho^* = 0.69$, however, τ decreases until $R_c = 3.5\sigma$ and then remains approximately constant. On a microscopic length scale, of course, the line tension should be interpreted with care.[44] This is partially due to the diffuse nature of the interface, which makes the identification of a three-phase contact line, hence estimating its length, difficult. Other effects, such as curvature corrections to the interfacial and surface tensions or terms related to the rigidity of the interface and stiffness of the contact line, may also affect the stability of particles at interfaces. The quantity τ appearing in Eq. (8) may be regarded as a correction factor dependent that depends on the line tension and the role of line tension on the stability of nanoparticles at interfaces may only be fully determined through an independent calculation of the line tension.[45]

It should be noted that for small particles the radius R_c used in continuum theories (for example, in Eq. (7)) may not correspond to the radius of the particle. In particular, due to the finite size of the solvent particles the excluded volume due to the nanoparticle or, more importantly in the present case, the change in the interfacial area between the two solvent components, may be larger than would be expected from the value of R_c. The effective nanoparticle radius (R_c^{eff}) may be estimated from the solvent probability distribution function (Fig. 4). From these $R_c^{eff} = 2.9\sigma$ for $R_c = 2.5\sigma$ and $R_c^{eff} = 4.4\sigma$ for $R_c = 4\sigma$. Using these effective radii increases the detachment free energy (Table II), however, it is still somewhat smaller than the simulation value. Another possible reason for the discrepancy between the detachment energies calculated from simulation and by Pieranski theory is the neglect of dispersion forces in the latter. While this may

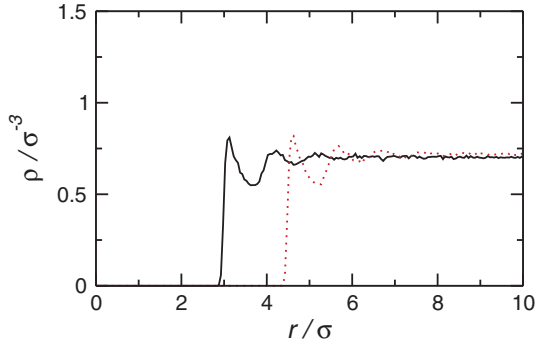

FIG. 4. Solvent density distributions around $R_c = 2.5\sigma$ (solid line) and $R_c = 4.0\sigma$ (dotted line) nanoparticles ($\beta\epsilon' = 0$) at solvent density $\rho^* = 0.69$.

indeed lead longer ranged and stronger interactions between the nanoparticle and the interface, previous simulation work on purely repulsive hard sphere systems[18] have shown a similar discrepancy, so dispersion forces are unlikely to be the primary reason for this. Additionally, while they are not explicitly included in continuum models, dispersion forces are implicitly included due to their contribution to interfacial and surface tensions in these theories.

B. Effect of attractive interactions

By changing ϵ' the effect of attractive interactions between the nanoparticle and solvent particles may be examined. Note that as the nanoparticle-solvent interaction remains identical for both solvent components the contact angle is constant ($\theta = \pi/2$). The effective potential as a function of ϵ' for $\rho^* = 0.50$ ($R_c = 2.5\sigma$ and 4σ) is shown in Fig. 5. On increasing ϵ' the detachment energy decreases. This may be understood as the number of solvent particles close to the nanoparticle (hence in the attractive potential well) is lower

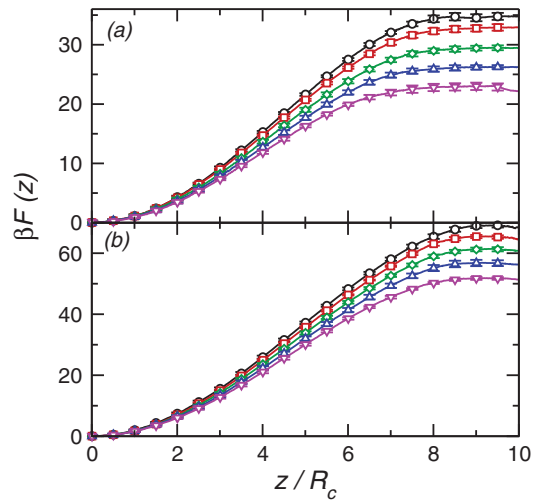

FIG. 5. (a) Free energy profile for $R_c = 2.5\sigma$ nanoparticle at solvent density $\rho^* = 0.50$. Circles (black) denote $\beta\epsilon' = 0$, squares (red) $\beta\epsilon' = 0.25$, diamonds (green) $\beta\epsilon' = 0.5$, triangles (blue) $\beta\epsilon' = 0.75$, and inverted triangles (magenta) $\beta\epsilon' = 1$. (b) Free energy profile for $R_c = 4\sigma$ nanoparticle at solvent density $\rho^* = 0.50$. Symbols as in (a).

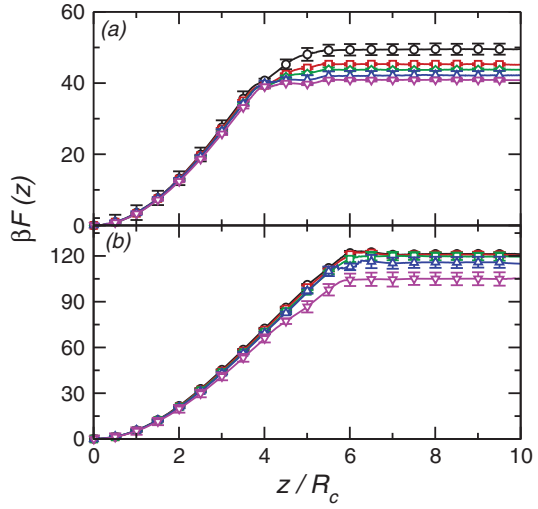

FIG. 6. (a) Free energy profile for $R_c = 2.5\sigma$ nanoparticle at solvent density $\rho^* = 0.69$. Circles (black) denote $\beta\epsilon' = 0$, squares (red) $\beta\epsilon' = 0.25$, diamonds (green) $\beta\epsilon' = 0.5$, triangles (blue) $\beta\epsilon' = 0.75$, and inverted triangles (magenta) $\beta\epsilon' = 1$. (b) Free energy profile for $R_c = 4\sigma$ nanoparticle at solvent density $\rho^* = 0.69$. Symbols as in (a).

at the interface, due to the depletion region between the two solvent components, than in the bulk solvent. At higher solvent density (Fig. 6), the behaviour of $F(z)$ on increasing ϵ' is the same. For the $R_c = 4\sigma$ nanoparticle, the small barrier that is present for $\epsilon' = 0$ disappears as ϵ' increases.

The variation in ΔF with ϵ' for all ρ^* studied is shown in Fig. 7. In all cases ΔF decreases with ϵ'. For $\rho^* = 0.50$, the decrease with ϵ' is approximately linear. On increasing ρ^*, however, the variation with ϵ' is more complex. For the $R_c = 4\sigma$ nanoparticle at $\rho^* = 0.69$ ΔF is approximately constant for $\beta\epsilon' \leq 0.25$ before decreasing. In order to determine the contribution of the potential energy to ΔF the difference between the average nanoparticle-solvent interaction energies,

$$\langle E_c \rangle = \left\langle \sum_{i=1}^{N_{solvent}} V_{SN}(|\boldsymbol{r}_c - \boldsymbol{r}_i|) \right\rangle, \tag{9}$$

where $V_{SN}(r)$ is given in Eq. (4) and the angled brackets denote an average over a simulation run, for nanoparticle constrained at $z_c = 0$ (interface) and $z_c = 9\sigma$ (bulk) were calculated (Table III). Apart from $\beta\epsilon' = 0$, $\Delta E_C = E_c(z = 9\sigma) - E_c(z = 0)$ is negative, indicating that attractive nanoparticle-solvent interactions lead to a destabilisation of the nanoparticle from the interface. Generally this accounts for a substantial proportion of the change in ΔF with ϵ' (for $\rho^* = 0.50$ and $R_c = 2.5\sigma$, the difference between ΔF for $\beta\epsilon' = 1$ and $\beta\epsilon' = 0$ is $\sim 11\ k_B T$, while the difference between ΔE_C is $\sim 7\ k_B T$). By contrast, the difference between the average interaction energy (E_{AB}) between the unlike components,

$$\langle E_{AB} \rangle = \left\langle \sum_{i=1}^{N_A} \sum_{j=1}^{N_B} V_S(|\boldsymbol{r}_i - \boldsymbol{r}_j|) \right\rangle, \tag{10}$$

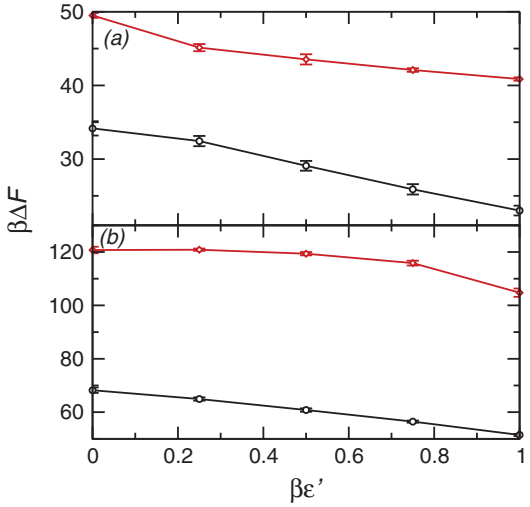

FIG. 7. (a) Detachment energy against ϵ' for $R_c = 2.5\sigma$ nanoparticle at solvent densities $\rho^* = 0.50$ (circles, black) and $\rho^* = 0.69$ (diamonds, red). (b) Detachment energy against ϵ' for $R_c = 2.5\sigma$ nanoparticle. Symbols as in (a).

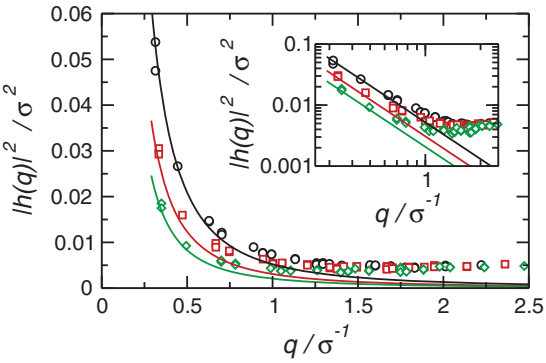

FIG. 8. Mean-squared Fourier components of the interface position $\langle|h(\boldsymbol{q})|^2\rangle$ for $\rho^* = 0.50$ (circles, black), $\rho^* = 0.60$ (squares, red), and $\rho^* = 0.69$ (diamonds, green). Lines show predictions of capillary wave theory. The inset shows the same data on a log-log plot.

for $z_c = 0$ and $z_c = 9\sigma$ (ΔE_{AB}) shows no clear trend with ϵ'. This is expected as, at fixed R_c, the change in interfacial area between the A and B components is the same for all ϵ'. The remaining contribution to ΔF may arise from entropic effects due to changes in solvent structure around the nanoparticle, both at the interface and in bulk solvent.

C. Capillary waves

One of the underlying assumptions of continuum approximations such as Pieranski theory, is that the interface is sharp and flat. On the microscopic level, the interface is broadened by bulk density fluctuations and thermal fluctuations in the interface position (capillary waves).[46] Central to the microscopic description of interfaces is the notion of a local interface position $h(\boldsymbol{r})$ ($\boldsymbol{r} = (x, y)$), which is often more conveniently described through its two-dimensional Fourier transform $h(\boldsymbol{q})$. In particular, capillary wave theory (CWT) predicts that at low q the mean-squared amplitudes of $h(\boldsymbol{q})$ varies as[47]

$$\langle|h(\boldsymbol{q})|^2\rangle = \frac{1}{\gamma\beta L_x^2 q^2}, \tag{11}$$

with $q = |\boldsymbol{q}|$. The plots of $\langle|h(\boldsymbol{q})|^2\rangle$ for the three densities studied in this work are shown in Fig. 8. At low-q $\langle|h(\boldsymbol{q})|^2\rangle$ indeed displays the $1/q^2$ behaviour predicted by capillary wave theory (although due to the finite size of the simulation box, only wavevectors with $q > 2\pi/L_x$ may be studied). At higher q deviations from CWT are seen, due to bulk density fluctuations.

TABLE III. Average nanoparticle (E_c) and A-B interaction (E_{AB}) energies for $z_c = 0$ and $z_c = 9\sigma$. Statistical errors in the final digit, estimated from the standard error of 50 000 measurements given in parenthesis.

ρ^*	R_c/σ	$\beta\epsilon'$	$\langle\beta E_c(z=0)\rangle$	$\langle\beta E_{AB}(z=0)\rangle$	$\langle\beta E_c(z=9\sigma)\rangle$	$\langle\beta E_{AB}(z=9\sigma)\rangle$	$\beta\Delta E_C$	$\beta\Delta E_{AB}$
		0.00	0.494(3)	12.74(2)	0.823(3)	11.37(2)	0.329(6)	− 1.38(4)
		0.25	− 1.518(3)	12.87(2)	− 2.368(4)	11.79(2)	− 0.850(9)	− 1.08(4)
0.50	2.5	0.50	− 4.182(4)	10.85(2)	− 6.773(5)	11.29(2)	− 2.591(9)	0.44(4)
		0.75	− 7.921(6)	12.11(2)	− 12.263(7)	13.68(2)	− 4.34(1)	1.57(4)
		1.00	− 12.609(9)	10.54(2)	− 19.170(9)	13.11(2)	− 6.56(2)	2.57(4)
		0.00	5.643(5)	10.19(2)	6.122(6)	10.80(2)	0.48(1)	− 0.61(4)
		0.25	− 3.262(4)	11.52(2)	− 4.442(5)	11.55(2)	− 1.180(9)	0.03(4)
0.50	4.0	0.50	− 9.353(6)	10.70(2)	− 12.761(8)	12.09(2)	− 3.41(1)	1.38(4)
		0.75	− 17.33(1)	10.31(2)	− 23.42(1)	13.93(2)	− 6.09(2)	3.62(4)
		1.00	− 31.63(1)	11.90(2)	− 41.09(1)	12.60(2)	− 9.46(2)	0.62(4)
		0.00	2.460(5)	19.36(2)	3.140(6)	19.80(2)	0.68(1)	0.44(3)
		0.25	− 3.325(4)	18.06(2)	− 3.612(4)	21.77(2)	− 0.287(9)	3.71(4)
0.69	2.5	0.50	− 9.919(6)	18.72(2)	− 11.061(7)	21.61(2)	− 1.14(1)	2.79(4)
		0.75	− 17.095(7)	18.19(2)	− 19.214(8)	20.18(2)	− 2.12(1)	1.99(4)
		1.00	− 25.048(9)	18.69(2)	− 27.990(9)	21.26(2)	− 2.94(2)	2.57(4)
		0.00	6.260(9)	18.41(2)	7.358(9)	23.31(2)	1.10(2)	4.90(4)
		0.25	− 7.027(9)	18.51(2)	− 7.340(9)	22.82(2)	− 0.29(2)	4.31(4)
0.69	4.0	0.50	− 21.93(1)	18.32(2)	− 23.72(1)	23.94(2)	− 1.79(2)	5.62(4)
		0.75	− 38.36(1)	19.20(2)	− 41.43(1)	23.39(2)	− 3.08(2)	4.19(4)
		1.00	− 58.79(2)	18.42(3)	− 63.30(2)	21.69(3)	− 4.51(4)	3.27(5)

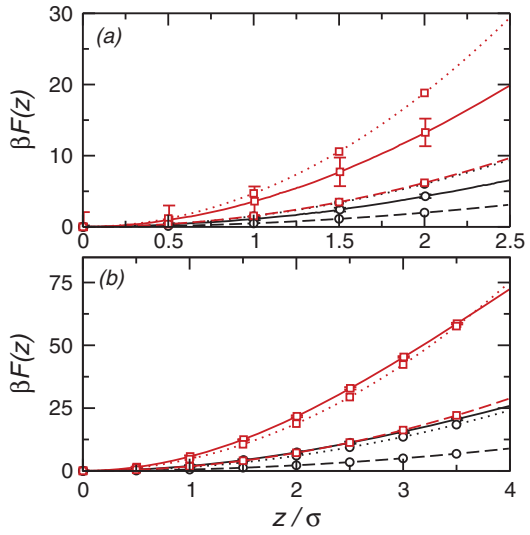

FIG. 9. (a) Effective nanoparticle-interface interaction for $R_c = 2.5\sigma$ nanoparticle at $\rho^* = 0.50$ (circles, black) and $\rho^* = 0.69$ (squares, red). Solid line denotes simulation results, dotted line Pieranski theory, and dashed line Lehle-Oettel expression. (b) Effective nanoparticle-interface interaction for $R_c = 4.0\sigma$ nanoparticle. Symbols at in (a).

Recently Lehle and Oettel (LO) calculated a correction to the Pieranski expression using a perturbative approach.[12] Within this approach the effective nanoparticle-interface interaction is given by

$$F_{\mathrm{LO}}(z_c) = \pi\gamma_{AB}(z_c - z_0)^2 \frac{1 - \frac{\hat{\tau}}{\hat{r}^3_{0,eq}}}{1 + \ln\hat{\lambda}_c\left(1 - \frac{\hat{\tau}}{\hat{r}_{0,eq}}\right)} \tag{12}$$

where $\hat{\tau} = \tau/(\gamma_{AB}R_c)$ is the reduced line tension, $r_{0,eq} = \sqrt{R_c^2 - z_{eq}^2}$ is the radius of the contact line (for $z = z_{eq}$), and $\hat{\lambda}_c \approx 1.12\lambda_c/r_{0,eq}$ is the reduced capillary length. Here, λ_c is effectively the largest capillary wave in the system; for gravitational systems $\lambda_c = \sqrt{\gamma_{AB}/(\Delta\rho g)}$, where g is the acceleration due to gravity and $\Delta\rho$ is the difference in mass density between the two phases, while in this case $\lambda_c = L_x$ (transverse box length).

Comparison between the effective potentials found from simulation and calculated using Eqs. (7) (Pieranski approximation) and (12) is shown in Fig. 9. For $R_c = 2.5\sigma$ nanoparticle the effective potential from simulation falls between the two theoretical predictions, with results from Eq. (7) lying above and Eq. (12) lying below the simulation curve. This may be understood as interface fluctuations lead to a more diffuse interface than assumed in Pieranski theory, so taking these into account leads to a softer interaction. For negative τ, as in this work, the effective potential from Eq. (2) varies more rapidly than the effective potential from the Pieranski approximation.[18] For $R_c = 4\sigma$ nanoparticle both the Pieranski and LO expressions give effective potentials that lie below the simulation results, with the potential from LO expression lying further from the simulation potential. In this case, the poor performance of the LO equation is likely due to the assumption, made in its derivation that $R_c \ll \lambda_c$ is in valid (for the $R_c = 4\sigma$ nanoparticle $\lambda_c/R_c \approx 4 - 5$) and simulations of larger systems would be needed to test its applicability.

TABLE IV. Line tensions and spring constants for $\epsilon' = 0$ nanoparticle. Numbers in parenthesis give errors in final digits.

ρ^*	R_c/σ	$\beta\sigma\tau$	$\beta\sigma^2 k_{sim}$	$\beta\sigma^2 k_{\mathrm{Pier}}$	$\beta\sigma^2 k_{\mathrm{AC}}$	$\beta\sigma^2 k_{LO}$
0.50	2.5	−1.58	2.068	3.014	3.27(1)	2.130(2)
	3.0	−1.66	2.341	3.014	3.143(2)	2.1246(4)
	3.5	−1.71	2.478	3.014	3.086(1)	2.1100(3)
	4.0	−1.76	2.799	3.014	3.057(1)	2.1085(2)
0.69	2.5	−1.28	5.770	9.412	9.619(3)	4.0640(7)
	3.0	−1.74	6.542	9.412	9.547(1)	4.4739(2)
	3.5	−1.84	7.010	9.412	9.489(1)	4.6106(1)
	4.0	−1.81	8.502	9.412	9.457(1)	4.6765(3)

The softening of the potential may be quantified through the (anharmonic) spring constant,

$$k = \left.\frac{d^2V}{dz^2}\right|_{z=0}, \tag{13}$$

which in the case of the Pieranski,[8] AC, and LO approximations are[12]

$$k_{\mathrm{Pier}} = 2\pi\gamma_{AB}, \tag{14a}$$

$$k_{\mathrm{AC}} = 2\pi\gamma_{AB}\left(1 - \hat{\tau}/\hat{r}^3_{0,eq}\right), \tag{14b}$$

$$k_{\mathrm{LO}} = 2\pi\gamma_{AB}\frac{1-\hat{\tau}/\hat{r}^3_{0,eq}}{1+\log\left(\hat{\lambda}\left(1-\hat{\tau}/\hat{r}^3_{0,eq}\right)\right)} \tag{14c}$$

(note that k_{Pier} is independent of R_c). k_{sim} is estimated from fitting a quadratic function to the region $z \le 2\sigma$. The collected values of k are given in Table IV. For both $\rho^* = 0.50$ and $\rho^* = 0.69$, k_{sim} increases with R_c. The inclusion of line tension has only a small effect on k, with the difference between k_{Pier} and k_{AC} decreasing as R_c increases; the line tension contribution to k_{AC} decreases as R_c^{-4} (Eq. (14b)). The behaviour of k_{LO} is quite different at low and high density. For $\rho^* = 0.50$, it decreases very slightly with R_c. At $\rho^* = 0.69$, however, there is a substantial increase in k_{LO} with R_c in agreement with simulation.

IV. CONCLUSIONS

In this paper, molecular dynamics simulations have been used to calculate the effective interaction between a spherical nanoparticle and a liquid-liquid interface in a binary Lennard-Jones fluid. The effective interaction is qualitatively similar to that calculated previously for hard sphere systems,[18] although the detachment free energy is significantly larger (of the order of 10–100 $k_{\mathrm{B}}T$ rather than 1–10 $k_{\mathrm{B}}T$) due to the larger interfacial tension. As before comparison between simulation and the continuum Pieranski approximation shows that the latter underestimates the strength and range of the interaction. The difference between simulation and Pieranski theory may arise due to its neglect of line tension and microscopic effects, such as capillary waves.

On including an attractive interaction between the nanoparticle and solvent particles, the detachment energy of

the nanoparticle decreases. This is as there are fewer close contacts between the nanoparticle and solvent particles when the nanoparticle is at the interface than when it is in bulk solvent. In the case studied here, when the contact angle $\theta = \pi/2$ the detachment energy from Pieranski theory remains unchanged with the attraction strength. Calculation of the change in the average nanoparticle-solvent interaction energies for nanoparticles at the interface and in bulk solvent shows that this accounts for a significant proportion of ΔF. The remainder of the change in ΔF may arise from entropic contributions due to rearrangement of the particles around the nanoparticle.

One of the underlying assumptions of the Pieranski approximation (and other continuum theories) is that the interface is sharp and flat. This leads to an interaction potential that for small particles varies too rapidly near the interface. The inclusion of capillary waves into the effective potential leads to a noticeable softening of the potential, as shown by a large decrease in the spring constant.

Overall it has been shown that the results previously obtained using MC simulations on an idealised fluid also hold for more realistic models. Future work may address the origin of the free energy barrier to adsorption seen for larger nanoparticle (Fig. 2) and the effect of capillary waves on the effect interaction. The method can also be applied to more complex nanoparticles, such as anisotropic or polymer tethered nanoparticles.

ACKNOWLEDGMENTS

The author is grateful to Dr. Fernando Bresme for helpful comments. This work was funded by ERC, University of Warwick and the Leverhulme trust (ECF/2010/0254). Computational resources were provided by the Centre for Scientific Computing, University of Warwick.

[1]F. Bresme and M. Oettel, J. Phys. Condens. Matter **19**, 413101 (2007).
[2]W. H. Binder, Angew. Chem., Int. Ed. **44**, 5172 (2005).
[3]S. Cauvin, P. J. Colver, and S. A. F. Bon, Macromolecules **38**, 7887 (2005).
[4]P. S. Clegg, J. Phys. Condens. Matter **20**, 113101 (2008).
[5]M. B. Linder, Curr. Opin. Colloid Interface Sci. **14**, 356 (2009).
[6]J. T. Russell, Y. Lin, A. Böker, L. Su, P. Carl, H. Zettl, J. He, K. Sill, R. Tangirala, T. Emrick, K. Littrell, P. Thiyagarajan, D. Cookson, A. Fery, Q. Wang, and T. P. Russell, Angew. Chem., Int. Ed. **44**, 2420 (2005).
[7]P. Finkle, H. D. Draper, and J. H. Hildebrand, J. Am. Chem. Soc. **45**, 278 (1923).
[8]P. Pieranski, Phys. Rev. Lett. **45**, 569 (1980).
[9]B. P. Binks and S. O. Lumsdon, Langmuir **16**, 8622 (2000).
[10]B. P. Binks and J. H. Clint, Langmuir **18**, 1270 (2002).
[11]R. Aveyard and J. H. Clint, J. Chem. Soc., Faraday Trans. **92**, 85 (1996).
[12]H. Lehle and M. Oettel, J. Phys. Condens. Matter **20**, 404224 (2008).
[13]M. Oettel and S. Dietrich, Langmuir **24**, 1425 (2008).
[14]H. Lehle, M. Oettel, and S. Dietrich, EPL **75**, 174 (2006).
[15]F. Bresme and N. Quirke, Phys. Rev. Lett. **80**, 3791 (1998).
[16]F. Bresme and N. Quirke, J. Chem. Phys. **110**, 3536 (1999).
[17]F. Bresme and N. Quirke, Phys. Chem. Chem. Phys. **1**, 2149 (1999).
[18]D. L. Cheung and S. A. F. Bon, Phys. Rev. Lett. **102**, 066103 (2009).
[19]D. L. Cheung and S. A. F. Bon, Soft Matter **5**, 3969 (2009).
[20]R. J. K. Udayana Ranatunga, R. J. B. Kalescky, C.-c. Chiu, and S. O. Nielsen, J. Phys. Chem. C **114**, 12151 (2010).
[21]F. Bresme, H. Lehle, and M. Oettel, J. Chem. Phys. **130**, 214711 (2009).
[22]L. L. Dai, R. Sharma, and C.-Y. Wu, Langmuir **21**, 2641 (2005).
[23]Y. Song, M. Luo, and L. L. Dai, Langmuir **26**, 5 (2010).
[24]D. L. Cheung, Chem. Phys. Lett. **495**, 55 (2010).
[25]P. Hopkins, A. J. Archer, and R. Evans, J. Chem. Phys. **131**, 124704 (2009).
[26]M. Zeng, J. Mi, and C. Zhong, Phys. Chem. Chem. Phys. **13**, 3932 (2011).
[27]B. Widom and J. S. Rowlinson, J. Chem. Phys. **52**, 1670 (1970).
[28]M. Oettel, A. Domingeuz, and S. Dietrich, Phys. Rev. E **71**, 051401 (2005).
[29]Y.-M. Ban, R. Tasseff, and D. Kopelevich, Mol. Simul. **37**, 525 (2011).
[30]M. E. Flatte, A. A. Kornyshev, and M. Urbakh, J. Phys. Condens. Matter **20**, 073102 (2008).
[31]F. Wang and D. Landau, Phys. Rev. Lett. **86**, 2050 (2001).
[32]G. Torrie and J. Valleau, J. Comput. Phys. **23**, 187 (1977).
[33]S. Park and K. Schulten, J. Chem. Phys. **120**, 5946 (2004).
[34]A. Laio and F. L. Gervasio, Rep. Prog. Phys. **71**, 126601 (2008).
[35]E. Darve, D. Rodríguez-Gómez, and A. Pohorille, J. Chem. Phys. **128**, 144120 (2008).
[36]R. Everaers and M. Ejtehadi, Phys. Rev. E **67**, 041710 (2003).
[37]P. J. in't Veld, M. K. Petersen, and G. S. Grest, Phys. Rev. E **79**, 021401 (2009).
[38]S. Kumar, J. M. Rosenberg, D. Bouzida, R. H. Swendsen, and P. A. Kollman, J. Comput. Chem. **13**, 1011 (1992).
[39]S. Plimpton, J. Comp. Phys. **117**, 1 (1995); see http://lammps.sandia.gov.
[40]W. G. Hoover, Phys. Rev. A **31**, 1695 (1985).
[41]J. H. Irving and J. G. Kirkwood, J. Chem. Phys. **18**, 817 (1950).
[42]K. Du, E. Glogowski, T. Emrick, T. P. Russell, and A. D. Dinsmore, Langmuir **26**, 12518 (2010).
[43]B. P. Binks, Curr. Opin. Colloid Interface Sci. **7**, 21 (2002).
[44]L. Schimmele, M. Napiorkowski, and S. Dietrich, J. Chem. Phys. **127**, 164715 (2007).
[45]Y. Djikaev, J. Chem. Phys. **123**, 184704 (2005).
[46]K. Mecke and S. Dietrich, Phys. Rev. E **59**, 6676 (1999).
[47]S. A. Safran, *Statistical Thermodynamics of Surfaces, Interfaces, and Membranes* (Persus, Cambridge, 1994).